In Situ Fabrication of Highly Conductive Metal Nanowire Networks with High Transmittance from Deep-Ultraviolet to Near-Infrared

Chunxiong Bao,[†,⊥] Jie Yang,[†,⊥] Hao Gao,[†] Faming Li,[†] Yingfang Yao,[‡] Bo Yang,[‡] Gao Fu,[†] Xiaoxin Zhou,[†] Tao Yu,[*,†,§] Yiqiang Qin,[‡] Jianguo Liu,[‡] and Zhigang Zou[†,§]

[†]National Laboratory of Solid State Microstructures, Eco-Materials and Renewable Energy Research Center (ERERC), Department of Physics, [‡]Collage of Engineering and Applied Science, and [§]Collaborative Innovation Center of Advanced Microstructures, Nanjing University, Nanjing 210093, China. [⊥]These authors contributed equally to the work.

ABSTRACT We have developed a facile and compatible method to *in situ* fabricate uniform metal nanowire networks on substrates. The as-fabricated metal nanowire networks show low sheet resistance and high transmittance (2.2 Ω sq^{-1} at $T = 91.1\%$), which is equivalent to that of the state-of-the-art metal nanowire networks. We demonstrated that the transmittance of the metal networks becomes homogeneous from deep-ultraviolet (200 nm) to near-infrared (2000 nm) when the size of the wire spacing increases to micrometer size. Theoretical and experimental analyses indicated that we can improve the conductivity of the metal networks as well as keep their transmittance by increasing the thickness of the metal films. We also carried out durability tests to demonstrate our as-fabricated metal networks having good flexibility and strong adhesion.

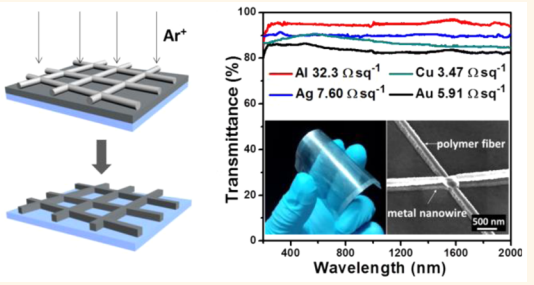

KEYWORDS: metal nanowire network · transparent conductive electrode · electrospinning · flexibility

Transparent conductive oxides (TCOs) such as indium tin oxide (ITO) (In_2O_3:Sn), fluorine-doped tin oxide (SnO_2:F), and aluminum-doped zinc oxide (ZnO:Al) have been widely used in optoelectronic devices as transparent electrodes. However, an inherent deficiency in these TCOs prevents their satisfactory application in some optoelectronic devices. For example, these TCOs cannot be effectively applied to ultraviolet (UV) and infrared (IR) detectors or solar cells with wide spectral absorption because the interband absorption and the light scattering by the free electrons can significantly decrease their transmittance in the UV and IR regions.[1] Moreover, the brittleness limits their applications in flexible optoelectronic devices.[2] Today, many kinds of novel materials, such as carbon nanotubes,[3−5] graphene,[6−8] conductive polymers,[9−11] and metal networks,[12−33] have been developed to meet the requirements of optoelectronic devices more widely. In these materials, the performance of the carbon-based materials and the polymers are limited by their low conductivity, although their flexibility can be improved significantly. The metal network is an important candidate to replace TCO as a transparent conductive electrode due to its excellent conductivity, flexibility, as well as its process compatibility in low-cost manufacturing techniques. Generally, there are two methods to form the metal networks. One method is randomly dispersing the metal nanowires on the substrates. The metal nanowires, such as Ag or Au, are usually fabricated by wet chemistry methods.[12−14] It is a facile way to obtain the metal network, but there are two disadvantages that restrict the conductivity, the lower length to diameter ratio of nanowires, and the higher wire-to-wire junction resistances.[34] Though some post-treatments, such as heating,[12,15] mechanical pressing,[16] plasmonic welting,[17] and

* Address correspondence to yutao@nju.edu.cn.

Received for review September 2, 2014 and accepted March 4, 2015.

Published online March 04, 2015
10.1021/nn504932e

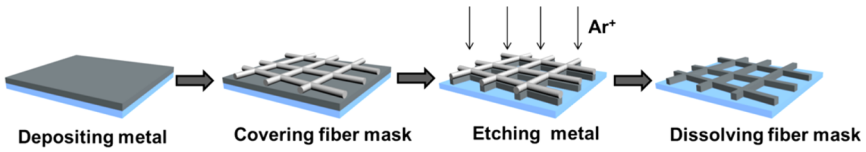

Figure 1. Schematic of the ion beam etching process with a polymer nanofiber network as the shadow mask to *in situ* fabricate a metal nanowire network on the substrate.

growing conductive materials on the junctions,[18−20] have been developed to reduce the junction resistances, the sheet resistances of the nanowire network electrodes are still relatively high (>20 Ω sq^{-1} at 90% transmittance). The other method is designing and patterning the metal thin films deposited by physical vapor deposition.[21−33] Metal networks fabricated by this method had higher conductivity due to the higher nanowires' conductivity and the elimination of the wire-to-wire junction resistances. However, most of these works were based on complex and high-cost processes such as nanoimprint lithography[21−24] or electron beam lithography,[25] which would increase the cost significantly. To decrease the fabrication cost, some low-cost materials and structures, such as electrospun polymer networks,[27,33] grain boundaries,[28] and film cracks,[29−32] have been introduced as pattern masks. Among them, electrospun polymer networks present remarkable performance due to their small and uniform diameter, ultralong fibers, and super connection. Cui's group fabricated transparent electrodes with high performance (sheet resistance 2 Ω sq^{-1} at 90% transmittance) by transferring the metal-deposited electrospun polymer networks to the substrates.[27] However, it is difficult to keep the metal network intact during the transfer processes, especially for large-area fabrication. Zhu's group developed a transfer-free method to fabricate Cu nanowire networks with electrospun polymer networks as a mask base in the solution etching process.[33] However, the performance of the Cu nanowire networks showed relatively low conductivity (sheet resistance 24 Ω sq^{-1} at 92% transmittance) because the solution etching process could generate defects on the networks. Therefore, how to prepare highly conductive and intact metal network electrodes by a facile and low-cost process remains a critical challenge.

In this work, we report a facile and compatible method to *in situ* fabricate metal nanowire networks on transparent substrates based on an ion beam etching (IBE) process with the electrospun polymer nanofiber networks as shadow masks. This method is a planar process quite similar to photolithography and is expected to be a compatible process in a production line to fabricate large-scale electrodes. The *in situ* method without a transfer process can keep the as-fabricated metal networks intact, which is significantly beneficial to the high performance of the metal nanowire networks. The as-fabricated metal nanowire networks have performance comparable to that of the state-of-the-art metal nanowire networks reported.[27] We also studied the optical properties of the metal nanowire networks. The optical simulations show that the transmittance of the networks becomes uniform from deep-UV to near-IR when the wire spacing increases to microscale, though the open ratio (OR) remains fixed. To our knowledge, this was rarely reported in previous work but is quite significant for UV and IR detectors or broad spectral range responsive solar cells. Furthermore, we performed durability experiments to confirm the performance of the as-fabricated metal nanowire networks under bending and abrasion conditions.

RESULTS AND DISCUSSION

Figure 1 shows the schematic of our method. At the beginning, a continuous metal layer was deposited on a transparent substrate by physical vapor deposition. Then an electrospun polymer nanofiber network as the shadow mask was covered on the surface of the as-deposited metal film. An IBE process was used to bombard and remove the metal that had not been covered by the polymer fibers. Finally, the remaining polymer fibers were dissolved by ethanol.

Figure 2a shows the optical microscopy image of the as-prepared Ag nanowire network on a glass substrate. The inset photograph shows the transparency of a sample of a 100 nm thick Ag nanowire network (T = 85%) on a glass substrate with a size of 2.5 cm × 2.5 cm. From the photograph, we can see the building clearly through the Ag nanowire network transparent electrodes (Supporting Information Figure S1 shows more photographs of the different metal nanowire network electrodes). The top view scanning electron microscopy (SEM) image (Figure 2b) of the Ag network indicates that the nanowires and network can remain intact on a large scale and the length/width ratio of the nanowire is large (~4 × 10^4), which is a benefit to reduce the sheet resistance of the whole metal network. SEM images of the Cu, Au, and Al networks on glass and the Ag network on the polyethylene terephthalate (PET) substrate are also shown in Figure S2. Figure 2c is the SEM image at a tilt angle of about 30° of the Ag nanowire network with the leftover polymer fiber mask. It indicates that the polymer fibers can effectively protect the bottom metal during the IBE process. Because IBE is an anisotropic process, the etching edge of the Ag nanowire is relatively sharp

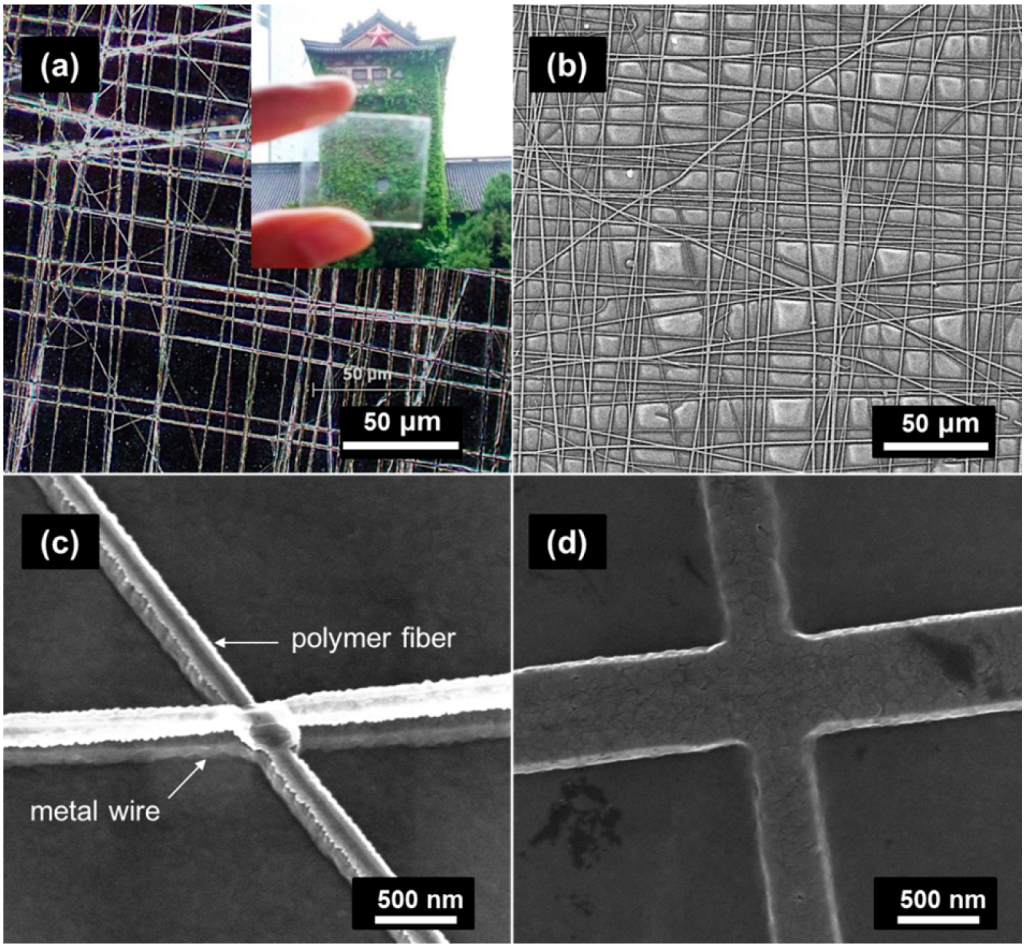

Figure 2. (a) Optical microscopy image of the Ag nanowire network on a glass substrate, with the polymer fiber network mask not dissolved. Inset is a photograph of the Ag nanowire network *in situ* fabricated on a 2.5 cm × 2.5 cm glass substrate. (b) Low-magnification SEM image of the Ag nanowire network on a glass substrate. (c) SEM image at a tilt angle of about 30° of the Ag nanowire network with the leftover fiber mask. (d) Enlarged SEM image of the interconnect section of the Ag wires.

and smooth, which is difficult to attain with the solution etching process.[33] The thickness of the Ag wire is about 100 nm, which is the same as that of the raw Ag film. Figure 2d shows the enlarged image at the intersection of Ag wires. The connection status will not produce the extra junction resistance, so that the sheet resistance of the whole network can be reduced effectively. This point is difficult to realize in the Ag nanowire networks that are assembled by a wet chemistry solution process. It can be found with careful observation that the edge of the Ag nanowires is not vertical but has a certain inclination. The reason is that the polymer fiber mask became thinner and its width became gradually narrower due to ion bombardment in the IBE process. Obviously, besides the metal nanowire networks, a various metal nanowire array can also be easily fabricated on different substrates *via* this method (Figure S3).

One of the advantages of the metal nanowire networks compared to a continuous metal oxide film is their broad transmission spectra. The continuous metal oxide films, such as ITO, usually present strong wavelength-selective transmittance when they are used as transparent conductive electrodes. This optical property is due to the interband absorption and the light scattering by the free electrons in the conduction band when the light has to transmit through the continuous film. If the metal nanowire networks can replace the continuous film, the transmittance property can be improved. The reason is that only the interaction between light and the free electrons in the metal can affect the transmittance because most of the light transmits through the open meshes on the networks. Although the metal nanowire network possesses broader transmission spectra compared to the continuous films, there is still a strong broad dip in the short wavelength due to the excitation of localized surface plasmon resonances (LSPRs) when a 2-D Ag nanowire network had a wire spacing of several hundred nanometers.[25,35] The simulation of 1-D Ag grid has drawn a conclusion that the transmission spectrum of the grid will fluctuate moderately and gradually approach the value of the open ratio (OR) when both the wire width and spacing increase (with fixed OR).[36] It is natural to deduce that, for a 2-D Ag nanowire network, when the wire spacing increases, the transmission

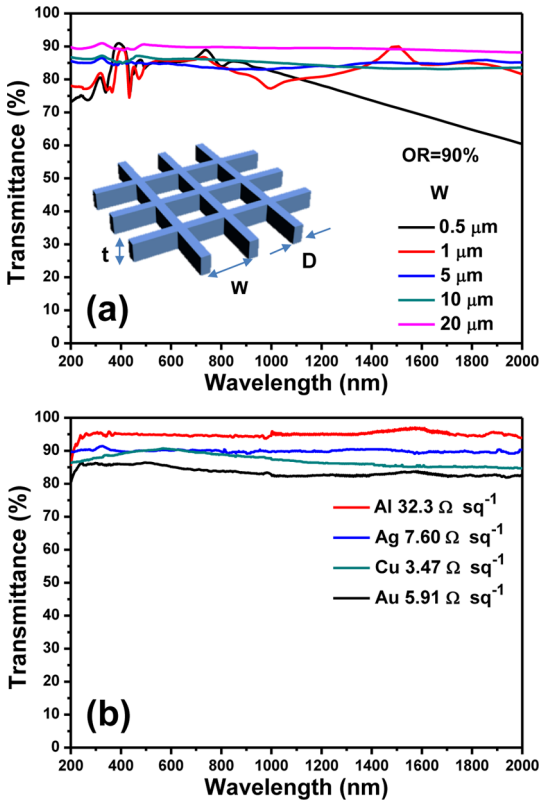

Figure 3. (a) Simulated optical transmission of 2-D Ag grids with an open ratio of 90% and different wire spacing. (b) Experimental optical transmission spectra of metal networks on quartz substrates.

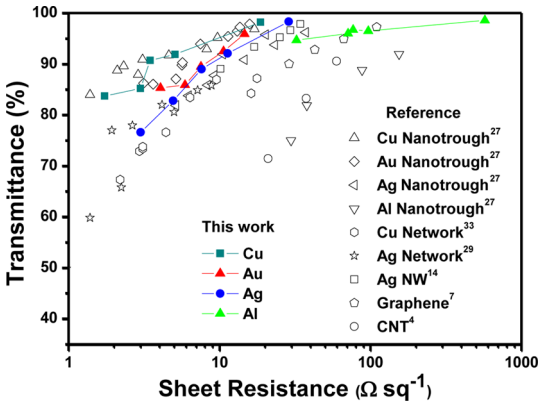

Figure 4. Optical transmission (at 550 nm) *versus* sheet resistance for our metal networks along with a metal nanotrough network,[27] Cu networks,[33] Ag networks,[29] Ag nanowire networks (Ag NW),[14] graphene,[7] and carbon nanotubes.[4]

spectra would change as that of the 1-D Ag grid. To confirm this point, we simulated the transmission spectrum of a Ag nanowire network by the finite difference time domain (FDTD) method.

In the simulation, the wire spacing (W) of the networks were chosen to be 0.5, 1, 5, 10, and 20 μm, and the wire widths (D) were 25.7, 51.3, 256.6, 513.2, and 1026 nm, respectively (with OR fixed at 90%); the thickness t was fixed at 100 nm. The network was posited on a SiO_2 substrate with thickness of 30 μm. A broad band (λ = 200−2000 nm) plane wave at normal incidence is used as a source, polarized along one of the Ag grid orientations. A power monitor was placed 500 nm above the Ag grid cell. Perfectly matched layer boundary conditions were used in the vertical direction, while periodic boundary conditions were used in both in-plane dimensions to simulate an infinite network. The optical constants of Ag and SiO_2 were obtained from a combined Drude, Lorentz, and Debye model fitted to the data from Palik. Figure 3a shows the results of the simulation. When the wire spacing is comparable to the wavelength (W = 0.5 or 1 μm), LSPRs lead to a transmittance dip in the short wavelength range, which is consistent with the experimental and simulated results reported in the previous work.[25,35] If the wire spacing increases and is greater than the wavelength (W = 5 and 10 μm), the transmission spectra become flat. When the spacing increases large enough (W = 20 μm), the transmission spectrum of the Ag network becomes a horizontal line approaching the value of OR. Figure 3b shows the experimental transmittance spectra of Al, Ag, Cu, and Au networks fabricated with our method. It demonstrates that all metal networks present high and homogeneous transmittance in the wavelength from 200 to 2000 nm. This implies that these metal networks can be effectively applied to the UV and IR detectors or the solar cell with wide spectral absorption since nearly one-fifth of the solar energy is in the wavelength from 1000 to 2000 nm of the AM1.5 solar spectrum.

The sheet resistances of the metal network transparent electrodes were tested with four probes. Figure 4 plots the optical transmittance (T) at 550 nm *versus* sheet resistances (R_S) of our Cu, Au, Ag, and Al nanowire networks as well as some results from previous reports. The sheet resistance values of our Cu, Au, Ag, and Al nanowire networks are 3.47 Ω sq^{-1} (T = 90.7%), 7.52 Ω sq^{-1} (T = 89.5%), 7.60 Ω sq^{-1} (T = 89.0%), and 76.7 Ω sq^{-1} (T = 96.7%) respectively. The performances of our metal nanowire networks are comparable or even better than that of metal nanotroughs,[27] Cu nanowire networks,[33] Ag networks,[29] Ag nanowire networks,[14] graphene,[7] and carbon nanotube[4] reported in the literature.

For a conventional continuous transparent conductive film, the performance can be explained by the bulk model:[37]

$$T = \left(1 + \frac{Z_0}{2R_S}\frac{\sigma_{OP}}{\sigma_{dc,B}}\right)^{-2} \quad (1)$$

where Z_0 is the impedance of free space (377 Ω), σ_{op} is the optical conductivity, $\sigma_{dc,B}$ is the bulk dc conductivity of the film. From eq 1, we can see there is a trade-off between the electrical conductivity and optical transmittance when the film thickness is diverse. Thicker layers offer lower sheet resistances but coupled with

lower optical transmittance and *vice versa*. Equation 1 also indicates that in order to improve the performance of the continuous film, the only way is to improve the material's property to obtain a higher optical conductivity or higher electrical conductivity. The case for the metal nanowire network with microscale wire spacing is quite different. The transmittance of the network is close to its OR:

$$T \approx \mathrm{OR} = \frac{(W - D)^2}{W^2} \quad (2)$$

where W is the wire spacing and D is the width of the metal wire. According to Kirchhoff's law, the sheet resistance R_S for a square $N \times N$ grid is given by[25]

$$R_S = \frac{N}{N+1}\frac{1}{\sigma_{dc,B}t}\frac{W}{D} \approx \frac{1}{\sigma_{dc,B}t}\frac{W}{D} \quad (3)$$

where t is the thickness of the film. The average widths of the as-fabricated Ag, Cu, and Au wires are 475.5, 450.0, and 1108.9 nm, respectively (Supporting Information Figure S4). The average wire spacing of the metal networks was estimated based on the SEM images (Figure S5). With the average width and wire spacing, we can calculate the transmittances and sheet resistances of the metal networks based on eqs 2 and 3. The calculated results as well as the measured results are displayed in Table S1. From the table, we can see that the calculated results agree well with the experimentally measured results.

By eliminating W/D, we can obtain a relationship between R_S and T from eqs 2 and 3:

$$R_S = [(1 - \sqrt{T})\sigma_{dc,B}t]^{-1} \quad (4)$$

The thickness t appears in eq 4 as an independent variable, which means that, besides the material's conductivity, we can also increase the thickness to improve the performance of the network. Figure 5 summarizes the experimental data of the Ag network with thicknesses of 100, 200, and 400 nm. When the thickness increases, the performance of the networks improves: the sheet resistance from 11.3 Ω sq^{-1} (T = 92.1%) for 100 nm to 3.84 Ω sq^{-1} (T = 91.25%) for 200 nm and 2.2 Ω sq^{-1} (T = 91.1%) for 400 nm. The lines in Figure 5 plot the relationship of eq 4 corrected by a factor σ: $R_S = \sigma[(1 - \sqrt{T})\sigma_{dc,B}t]^{-1}$, with the conductivity $\sigma_{dc,B} = 6.1 \times 10^7$ S m^{-1}. The correction factor σ for 100 and 200 nm thick networks is 2.5, and for a 400 nm thick network, it is 3.0. By introducing the correction factor σ, the simulated and experimental data were in agreement, which indicates that this grid model is effective to explain the Ag networks fabricated in this work. The correction factor σ may originate from the geometrical differences between the experimental network and the ideal grid model as well as the distinction of the film's real conductivity and the given bulk conductivity. One of the geometrical differences is that there exists an inclination in the experimental

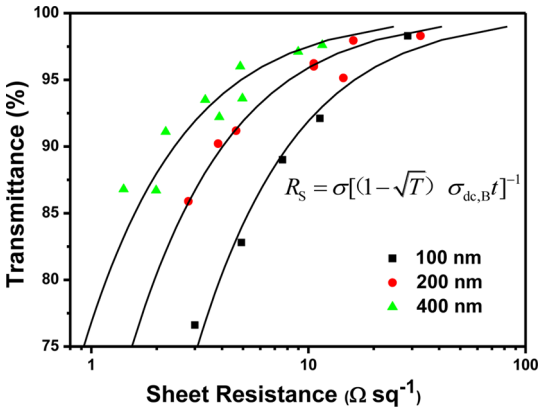

Figure 5. Optical transmission (at 550 nm) *versus* sheet resistance for our Ag nanowire network with thicknesses of 100, 200, and 400 nm. The symbols represent the experiment data. The lines represent the relation of the inserted equation with the correction factor σ = 2.5 for 100 and 200 nm thicknesses and σ = 3.0 for 400 nm thickness.

nanowire's edge wall, while the wire's wall in the grid model is vertical, so the experimental sheet resistances are always larger than the calculated results. Thicker metal films need longer etching time and form more tilted edge walls, which will lead to larger deviation between experimental and calculated results. We can conclude that, when the thickness of the film further increases in the experiment, the performance of the network will become better, but the deviation between experimental and calculated results will also become larger. We did not further increase the thickness in the experiment because the results of the three different thicknesses can already reflect this trend. In order to demonstrate the trend of the sheet resistance to decrease with the thickness, the plots of sheet resistance *versus* thickness at certain transmittance are shown in Figure S6.

Possessing outstanding flexibility is also one of the advantages of our metal networks compared to TCO. In this work, as an example, we performed the bending test of our Ag nanowire network. Figure 6a,b shows the results of the bending test, with photographs of the flexible electrode (5 cm × 6 cm in size) and the bending test system as insets. Figure 6a shows that, when bent to a bending radius from 100 mm to 1.2 mm (the strain is from 0.13 to 10.5%, strain = $(t_s + t_f)/2R_c$, where t_s, t_f, and R_c are the thickness of the substrate, the thickness of the network film, and the bending radius[7]), the sheet resistance of the Ag nanowire network had no obvious increase: less than 1.2% when the bending radius is 100 to 4 mm and less than 31% when the bending radius is 4 to 1.2 mm. In comparison, the sheet resistance of ITO on PET increases dramatically when the bending radius is shorter than 10 mm. Figure 6b exhibits the variations in sheet resistance of a Ag nanowire network electrode and an ITO electrode on the PET film as a function of the number of cycles of repeated bending to a radius of 10 mm (strain ≈ 1.25%). After

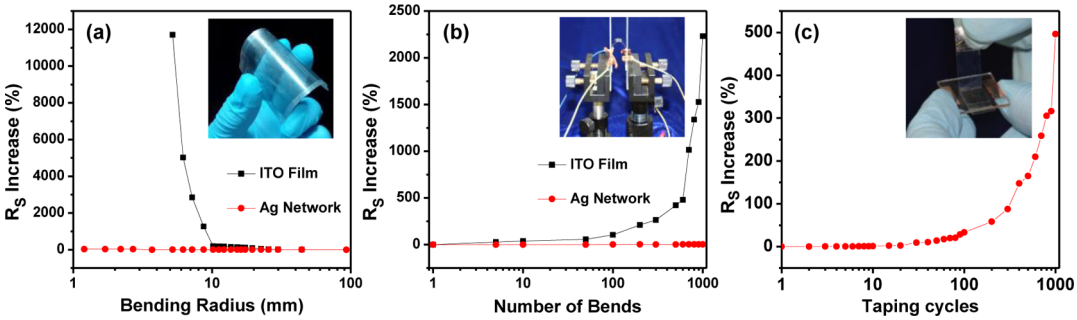

Figure 6. (a) Sheet resistance *versus* bending radius for flexible transparent electrodes consisting of a Ag network or ITO film on PET substrates. Inset is a photograph of the Ag network on a bent PET substrate. (b) Sheet resistance *versus* bending number (the repeated bending radius is ~10 mm, strain ≈ 1.25%) for flexible transparent electrodes consisting of a Ag network or ITO films on PET substrates. Inset is the photograph of the bending test instrument. (c) Sheet resistance *versus* the cycle numbers of taping and peeling.

1000 cycles of the bending test, the sheet resistance of the Ag network electrode increases less than 5% while the ITO electrode increases more than 20 times. The adhesion of the as-fabricated metal network to the substrate was also tested by attaching tape to the electrode and then peeling it off (inset of Figure 6c). From Figure 6c, we can see that, for Cu networks, the sheet resistance increases less than 35% when repeated attaching and peeling for 100 cycles. Unlike metal nanowire networks fabricated on substrates by a solution method or a transfer process, which always have poor adhesion, the *in situ* fabricated metal networks can adhere to substrates as tough as evaporated metal films. The atomic force microscope (AFM) topology image in Figure S7 also shows that the metal nanowires were firmly attached to the substrates. From the AFM image and cross section profile, we can see that the surface of our metal network electrode is relatively smooth compared to the solution-processed Ag nanowire network electrodes. Surface roughness is an important parameter for transparent electrodes depending on the application.[38] The root-mean-square surface roughness R_q calculated from five different cross section profiles are from 55 to 63 nm, which are smaller than that of Ag nanotrough network[27] and the Ag nanowire network[18] and comparable to that of Ag nanowire network after pressed with high pressure.[18]

The measurement and test results of our metal networks indicated that they possess high electrical conductivity and transmittance, as well as excellent flexibility and adhesion, which is favorable for their applications in optoelectronic devices. Herein, we fabricated photodetectors and a four-wire resistive touch screen working prototype as examples for the applications of our metal network electrodes. The photodetectors were fabricated by using organolead halide perovskite ($CH_3NH_3PbI_3$) as a photoactive layer, Au wire network electrodes and a Cu probe as bottom and top contact electrodes (inset of Figure 7b). The photodetectors were illuminated through the Au wire network electrode with monochromatic light, and the

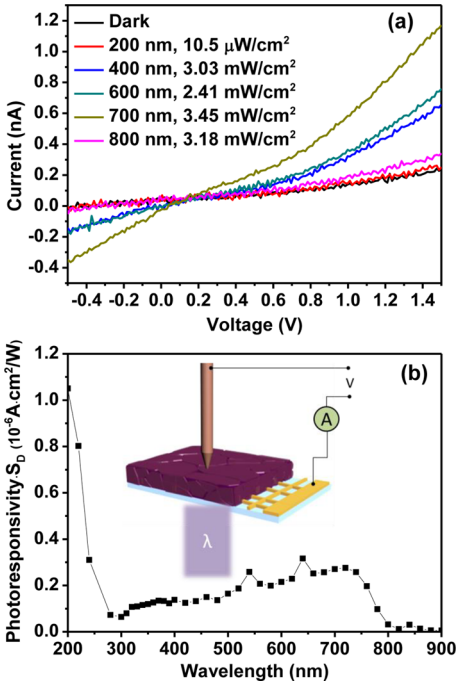

Figure 7. (a) *I*–*V* curves of the $CH_3NH_3PbI_3$ photodetector based on the Au wire network transparent electrode in the dark and illuminated by different monochromatic light. (b) Photoresponsivity of the photodetector *versus* the wavelengths of the illumination source. S_D in the ordinate represents the active area of the device.

photocurrents were measured with a sourcemeter. Figure 7a shows the *I*–*V* curves of one of our devices when in the dark and illuminated by different monochromatic light, and Figure 7b shows its spectral photoresponse at wavelengths from 200 to 900 nm at a bias of 1.5 V. Both the *I*–*V* curves and spectral photoresponse demonstrate that the Au wire network based photodetectors are effective for deep-UV light with a wavelength of 200 nm, which is beneficial from the high transmittance to deep-UV light of our metal network electrodes. To confirm the response of our photodetectors, the current characteristics at a bias of 1.5 V with the light switched on/off were studied, and the results are exhibited in Figure S8. The four-wire

resistive touch screen working prototype was fabricated by replacing the ITO bottom electrode of a commercial device with the Au network electrode on glass (Figure S9). Figure S10 shows the demonstration of writing with the touch screen connected to a computer, which indicates that our metal network electrodes have potential applications in touch screen devices.

CONCLUSION

In conclusion, the transparent conductive metal nanowire network electrodes have been successfully *in situ* fabricated on transparent substrates *via* an ion beam etching process with the electrospun polymer nanofiber networks as shadow masks. Due to the ultralarge length-to-width ratio, low wire-to-wire contact resistance, and the large wire spacing, which benefit from the fabrication method, the as-prepared electrodes have high conductivity as well as high and homogeneous transmittance from deep-UV to near-IR. The simulation and experimental results indicated that we can improve the transmittance and conductivity simultaneously by increasing the thickness of the network. We also demonstrate that the Ag nanowire network can retain good conductivity under repeated bending and abrasion operations. These metal nanowire network electrodes could replace ITO when applied in optoelectronic devices such as solar cells, touch screens, and especially flexible UV or IR devices.

METHODS

Deposition of Continuous Metal Films. The Cu, Au, Ag, and Al continuous films were deposited on glass, quartz (~1.0 mm in thickness), and PET (~0.25 mm in thickness) substrates by an electron beam evaporation system (Kurt J. Lesker, USA) at a base pressure of 1×10^{-6} Torr with the deposition rate at about 1 Å s^{-1}. In order to test the sheet resistance and deep-UV to near-IR transmittance, the films were deposited on a quartz substrate with a size of 1 cm × 2 cm.

Fabrication of an Electrospun Polymer Fiber Network Mask. PVP (MW: 1 300 000, Sigma-Aldrich) powder was dissolved in ethanol by continuous stirring for 2 h at room temperature to form a clear solution (14 wt %). The PVP solution was loaded in a 10 mL plastic syringe attached to a syringe pump, which provided a steady solution flow rate of 0.2 mL h^{-1} during electrospinning. PVP solution was spun from the needle onto a rectangle steel frame collector to form an aligned nanofiber array. During electrospinning, the voltage applied to the needle was 15 kV and the collector was kept grounded. The distance between the needle and the collector is ~25 cm. The electrospinning time was altered from 15 to 1 min to control the density of the collected polymer nanofibers. The collected polymer nanofiber array was then transferred to the top of the metal film. Repeated transfer process in the vertical direction formed a polymer nanofiber network on top of the metal film. To fabricate large-area electrodes, polymer nanowire network masks were collected on the metal film covered with electrodes directly.

Etching of the Metal Film. The etching process of the polymer nanofiber network covered metal film was carried out in an ion beam etching system (IBE150, Beijing Chuangshi Weina, China). The metal film electrodes were attached on a rotating stage with silicone grease. During etching, the rotating stage was kept vertical to the ion beam and rotated at a rate of 5 rpm. The ion beam was produced by a Kaufman-type ion source with argon (5.0 sccm) as the working gas. Before etching, the work chamber was kept at a base pressure of 8.0×10^{-4} Pa. To allow electrical characterization, a mask was covered on the electrode to limit the total size of the network to be 1 cm × 1 cm, and two electrical contact pads with a size of 1 cm × 0.5 cm were left.

Characterization. The morphologies of the networks were characterized by an optical microscope (Imager M1m, Zeiss, Germany), a SEM system (FEI NOVA NanoSEM230, USA), and an AFM system (MFP-3D-SA, Asylum Research, USA). The cross section profile of the network electrodes was tested using a profilometer (DEKTAK 150, Veeco Instruments Inc., USA). The transmittance spectra were measured with a Shimadzu UV 3600 UV−IR spectrophotometer. A bare quartz slide was used for reference. The measurements were carried out without an integrating sphere, so diffuse light and haze were not included. The sheet resistances were measured using a Keithley 2400 sourcemeter with four probes to eliminate contact resistance. To test the sheet resistance of the bending electrode on PET, four stripe-shaped contacts were made by conductive silver paint and connected to the sourcemeter with clips.

Photodetector and Touch Screen Device Fabrication. A Au network on quartz substrate electrodes ($R_S \sim 10\ \Omega\ sq^{-1}$, $T \sim 92\%$) was cleaned with ethanol and than treated with UV-ozone cleaner for 30 min. $CH_3NH_3PbI_3$ was fabricated on the Au network electrodes *via* two-step spin-coating and solvent annealing method.[39] Briefly, 450 mg/mL PbI_2 solution in dimethylformamide (DMF) and 45 mg/mL CH_3NH_3I solution in isopropyl alcohol were spin-coated on the cleaned Au network electrodes at 3000 rpm for 30 s in sequence. Then the samples were annealed in a DMF vapor atmosphere at 100 °C for 1 h. To measure the photocurrent, a Cu probe pressed on the perovskite film was used as one of the two electrodes and the Au network as the other one (inset of Figure 7b); a Keithley 2400 sourcemeter was used to test the photocurrent. The monochromatic lights were produced from a 1000 W Xe lamp through a monochromator (Omin-λ500, Zolix, China), and the power of the monochromatic lights was measured with a power meter (1918-C, Newport, USA). The measurements were performed in a black box with a background light power lower than 20 nW. A four-wire resistive touch screen device was rebuilt from a 3.0 in. commercial touch screen that consisted of a parallel ITO glass bottom electrode and an ITO PET top electrode. In this experiment, the ITO coating on glass was replaced with our Au network electrode on glass (Figure S9). The contact pads of the Au network electrode were formed with Ag paste. The circuit was connected with a computer and the performance tested by a commercial controller.

Conflict of Interest: The authors declare no competing financial interest.

Acknowledgment. We thank the financial support from the National Natural Science Foundation of China (11174129 and 61377051), the National Basic Research Program of China (2011CB933303 and 2013CB632404), the Jiangsu Provincial Science and Technology Research Program (BE2012089 and BK20130053), and the Scientific Research Foundation of Graduate School of Nanjing University (2014CL01). We thank K. Qiu, Z. Wang, Y. Zhou, and W. Tu for their experimental and technical assistance.

Supporting Information Available: Photographs and SEM images of the metal network transparent electrodes, distributions of metal wire widths, average wire spacing, the relation of R_S and thickness of Ag networks, and demonstration of the application in a photodetector and touch screen. This material is available free of charge *via* the Internet at http://pubs.acs.org.

REFERENCES AND NOTES

1. Deceglie, M. G.; Ferry, V. E.; Alivisatos, A. P.; Atwater, H. A. Design of Nanostructured Solar Cells Using Coupled Optical and Electrical Modeling. *Nano Lett.* **2012**, *12*, 2894–2900.

2. Chen, Z.; Cotterell, B.; Wang, W.; Guenther, E.; Chua, S. A Mechanical Assessment of Flexible Optoelectronic Devices. *Thin Solid Films* **2001**, *394*, 202–206.
3. Wu, Z.; Chen, Z.; Du, X.; Logan, J. M.; Sippel, J.; Nikolou, M.; Kamaras, K.; Reynolds, J. R.; Tanner, D. B.; et al. Transparent, Conductive Carbon Nanotube Films. *Science* **2004**, *305*, 1273–1276.
4. Li, J.; Hu, L.; Wang, L.; Zhou, Y.; Grüner, G.; Marks, T. J. Organic Light-Emitting Diodes Having Carbon Nanotube Anodes. *Nano Lett.* **2006**, *6*, 2472–2477.
5. Du, J.; Pei, S.; Ma, L.; Cheng, H.-M. 25th Anniversary Article: Carbon Nanotube- and Graphene-Based Transparent Conductive Films for Optoelectronic Devices. *Adv. Mater.* **2014**, *26*, 1958–1991.
6. Kim, K. S.; Zhao, Y.; Jang, H.; Lee, S. Y.; Kim, J. M.; Kim, K. S.; Ahn, J.-H.; Kim, P.; Choi, J.-Y.; Hong, B. H. Large-Scale Pattern Growth of Graphene Films for Stretchable Transparent Electrodes. *Nature* **2009**, *457*, 706–710.
7. Bae, S.; Kim, H.; Lee, Y.; Xu, X.; Park, J.-S.; Zheng, Y.; Balakrishnan, J.; Lei, T.; Kim, H. R.; Song, Y. I.; et al. Roll-to-Roll Production of 30-Inch Graphene Films for Transparent Electrodes. *Nat. Nanotechnol.* **2010**, *5*, 574–578.
8. Pang, S.; Hernandez, Y.; Feng, X.; Müllen, K. Graphene as Transparent Electrode Material for Organic Electronics. *Adv. Mater.* **2011**, *23*, 2779–2795.
9. Cao, Y.; Treacy, G. M.; Smith, P.; Heeger, A. J. Solution-Cast Films of Polyaniline: Optical-Quality Transparent Electrodes. *Appl. Phys. Lett.* **1992**, *60*, 2711–2713.
10. Yang, Y.; Heeger, A. J. Polyaniline as a Transparent Electrode for Polymer Light-Emitting Diodes: Lower Operating Voltage and Higher Efficiency. *Appl. Phys. Lett.* **1994**, *64*, 1245–1247.
11. Xia, Y.; Sun, K.; Ouyang, J. Solution-Processed Metallic Conducting Polymer Films as Transparent Electrode of Optoelectronic Devices. *Adv. Mater.* **2012**, *24*, 2436–2440.
12. Lee, J.-Y.; Connor, S. T.; Cui, Y.; Peumans, P. Solution-Processed Metal Nanowire Mesh Transparent Electrodes. *Nano Lett.* **2008**, *8*, 689–692.
13. De, S.; Higgins, T. M.; Lyons, P. E.; Doherty, E. M.; Nirmalraj, P. N.; Blau, W. J.; Boland, J. J.; Coleman, J. N. Silver Nanowire Networks as Flexible, Transparent, Conducting Films: Extremely High DC to Optical Conductivity Ratios. *ACS Nano* **2009**, *3*, 1767–1774.
14. Leem, D.-S.; Edwards, A.; Faist, M.; Nelson, J.; Bradley, D. D. C.; de Mello, J. C. Efficient Organic Solar Cells with Solution-Processed Silver Nanowire Electrodes. *Adv. Mater.* **2011**, *23*, 4371–4375.
15. Song, T.-B.; Chen, Y.; Chung, C.-H.; Yang, Y.; Bob, B.; Duan, H.-S.; Li, G.; Tu, K.-N.; Huang, Y.; Yang, Y. Nanoscale Joule Heating and Electromigration Enhanced Ripening of Silver Nanowire Contacts. *ACS Nano* **2014**, *8*, 2804–2811.
16. Tokuno, T.; Nogi, M.; Karakawa, M.; Jiu, J.; Nge, T. T.; Aso, Y.; Suganuma, K. Fabrication of Silver Nanowire Transparent Electrodes at Room Temperature. *Nano Res.* **2011**, *4*, 1215–1222.
17. Garnett, E. C.; Cai, W.; Cha, J. J.; Mahmood, F.; Connor, S. T.; Christoforo, M. G.; Cui, Y.; McGehee, M. D.; Brongersma, M. L. Self-Limited Plasmonic Welding of Silver Nanowire Junctions. *Nat. Mater.* **2012**, *11*, 241–249.
18. Hu, L.; Kim, H. S.; Lee, J.-Y.; Peumans, P.; Cui, Y. Scalable Coating and Properties of Transparent, Flexible, Silver Nanowire Electrodes. *ACS Nano* **2010**, *4*, 2955–2963.
19. Lee, J.; Lee, P.; Lee, H. B.; Hong, S.; Lee, I.; Yeo, J.; Lee, S. S.; Kim, T.-S.; Lee, D.; Ko, S. H. Room-Temperature Nanosoldering of a Very Long Metal Nanowire Network by Conducting-Polymer-Assisted Joining for a Flexible Touch-Panel Application. *Adv. Funct. Mater.* **2013**, *23*, 4171–4176.
20. Lu, H.; Zhang, D.; Ren, X.; Liu, J.; Choy, W. C. H. Selective Growth and Integration of Silver Nanoparticles on Silver Nanowires at Room Conditions for Transparent Nanowire Network Electrode. *ACS Nano* **2014**, *8*, 10980–10987.
21. Kang, M.-G.; Guo, L. J. Nanoimprinted Semitransparent Metal Electrodes and Their Application in Organic Light-Emitting Diodes. *Adv. Mater.* **2007**, *19*, 1391–1396.
22. Kang, M.-G.; Guo, L. J. Semitransparent Cu Electrode on a Flexible Substrate and Its Application in Organic Light Emitting Diodes. *J. Vac. Sci. Technol., B* **2007**, *25*, 2637–2641.
23. Kang, M.-G.; Kim, M.-S.; Kim, J.; Guo, L. J. Organic Solar Cells Using Nanoimprinted Transparent Metal Electrodes. *Adv. Mater.* **2008**, *20*, 4408–4413.
24. Kang, M.-G.; Park, H. J.; Ahn, S. H.; Guo, L. J. Transparent Cu Nanowire Mesh Electrode on Flexible Substrates Fabricated by Transfer Printing and Its Application in Organic Solar Cells. *Sol. Energy Mater. Sol. Cells* **2010**, *94*, 1179–1184.
25. van de Groep, J.; Spinelli, P.; Polman, A. Transparent Conducting Silver Nanowire Networks. *Nano Lett.* **2012**, *12*, 3138–3144.
26. Kuang, P.; Park, J.-M.; Leung, W.; Mahadevapuram, R. C.; Nalwa, K. S.; Kim, T.-G.; Chaudhary, S.; Ho, K.-M.; Constant, K. A New Architecture for Transparent Electrodes: Relieving the Trade-Off Between Electrical Conductivity and Optical Transmittance. *Adv. Mater.* **2011**, *23*, 2469–2473.
27. Wu, H.; Kong, D.; Ruan, Z.; Hsu, P.; Wang, S.; Yu, Z.; Carney, T. J.; Hu, L.; Fan, S.; Cui, Y. A Transparent Electrode Based on a Metal Nanotrough Network. *Nat. Nanotechnol.* **2013**, *8*, 421–425.
28. Guo, C. F.; Sun, T.; Liu, Q.; Suo, Z.; Ren, Z. Highly Stretchable and Transparent Nanomesh Electrodes Made by Grain Boundary Lithography. *Nat. Commun.* **2014**, *5*, 3121.
29. Han, B.; Pei, K.; Huang, Y.; Zhang, X.; Rong, Q.; Lin, Q.; Guo, Y.; Sun, T.; Guo, C.; Carnahan, D.; et al. Uniform Self-Forming Metallic Network as a High-Performance Transparent Conductive Electrode. *Adv. Mater.* **2014**, *26*, 873–877.
30. Kiruthika, S.; Gupta, R.; Rao, K. D. M.; Chakraborty, S.; Padmavathy, N.; Kulkarni, G. U. Large Area Solution Processed Transparent Conducting Electrode Based on Highly Interconnected Cu Wire Network. *J. Mater. Chem. C* **2014**, *2*, 2089–2094.
31. Rao, K. D. M.; Gupta, R.; Kulkarni, G. U. Fabrication of Large Area, High-Performance, Transparent Conducting Electrodes Using a Spontaneously Formed Crackle Network as Template. *Adv. Mater. Interfaces* **2014**, 1400090.
32. Rao, K. D. M.; Hunger, C.; Gupta, R.; Kulkarni, G. U.; Thelakkat, M. A Cracked Polymer Templated Metal Network as a Transparent Conducting Electrode for ITO-Free Organic Solar Cells. *Phys. Chem. Chem. Phys.* **2014**, *16*, 15107–15110.
33. He, T.; Xie, A.; Reneker, D. H.; Zhu, Y. A Tough and High-Performance Transparent Electrode from a Scalable and Transfer-Free Method. *ACS Nano* **2014**, *8*, 4782–4789.
34. Mutiso, R. M.; Sherrott, M. C.; Rathmell, A. R.; Wiley, B. J.; Winey, K. I. Integrating Simulations and Experiments To Predict Sheet Resistance and Optical Transmittance in Nanowire Films for Transparent Conductors. *ACS Nano* **2013**, *7*, 7654–7663.
35. Catrysse, P. B.; Fan, S. Nanopatterned Metallic Films for Use as Transparent Conductive Electrodes in Optoelectronic Devices. *Nano Lett.* **2010**, *10*, 2944–2949.
36. Lee, K.; Song, S. H.; Ahn, J. FDTD Simulation of Transmittance Characteristics of One-Dimensional Conducting Electrodes. *Opt. Express* **2014**, *22*, 6269–6275.
37. De, S.; Coleman, J. N. The Effects of Percolation in Nanostructured Transparent Conductors. *MRS Bull.* **2011**, *36*, 774–781.
38. Guo, C. F.; Ren, Z. Flexible Transparent Conductors Based on Metal Nanowire Networks. *Mater. Today* **2014**, 10.1016/j.mattod.2014.08.018.
39. Xiao, Z.; Dong, Q.; Bi, C.; Shao, Y.; Yuan, Y.; Huang, J. Solvent Annealing of Perovskite-Induced Crystal Growth for Photovoltaic-Device Efficiency Enhancement. *Adv. Mater.* **2014**, *26*, 6503–6509.